Available online at www.sciencedirect.com

ScienceDirect

Geochimica et Cosmochimica Acta 290 (2020) 124–136

Geochimica et Cosmochimica Acta

www.elsevier.com/locate/gca

Cadmium adsorption to clay-microbe aggregates: Implications for marine heavy metals cycling

Qixing Zhou [a,*], Yuxia Liu [b], Tian Li [a], Huazhang Zhao [c], Daniel S. Alessi [d], Weitao Liu [a], Kurt O. Konhauser [d]

[a] *Key Laboratory of Pollution Processes and Environmental Criteria (Ministry of Education), College of Environmental Science and Engineering, Nankai University, Tianjin 300350, China*

[b] *State Key Laboratory of Heavy Oil Processing, State Key Laboratory of Petroleum Pollution Control, China University of Petroleum, Beijing 102200, China*

[c] *Key Laboratory of Water and Sediment Sciences (Ministry of Education), College of Environmental Science and Engineering, Peking University, Beijing 100871, China*

[d] *Department of Earth and Atmospheric Sciences, University of Alberta, Edmonton, Alberta T6G 2E3, Canada*

Received 18 June 2020; accepted in revised form 3 September 2020; Available online 11 September 2020

Abstract

Interactions between microorganisms and clay minerals influence the transport and cycling of metal contaminants in both marine and terrestrial environments. The present study was conducted to quantify the adsorption of dissolved cadmium, Cd (II), under seawater-like conditions to the marine cyanobacterium *Synechococcus* sp. PCC 7002, three common clay minerals (kaolinite, montmorillonite and illite), as well as cell-clay aggregates. We show here that the *Synechococcus*-only experiments removed the most Cd above pH 5.5, followed in decreasing order by aggregates of 50% cells:50% individual clays, aggregates of cells and all 3 clays, and individual clays. Electron microscope imaging showed that clays associated in a tangential edge-on orientation to the cells in *Synechococcus*-clay mineral aggregates. A non-electrostatic surface complexation modeling approach was used to fit Cd adsorption onto *Synechococcus* cells and individual clay minerals. The resulting Cd binding constants were then used in consort with surface functional group p*K*a values and site concentrations to accurately predict the extent of Cd adsorption onto the *Synechococcus*-clay mineral aggregates using the component additivity (CA) approach. We observed that the addition of cyanobacterial cells to clay mineral suspensions led to significantly larger mean aggregate sizes of clay minerals, enhancing the clay sedimentation rate. Although specifically focused on Cd, our study indicates that the ratio of bacterial plankton to clay minerals is an important determinant in terms of understanding the rate with which metals are transferred from the water column to the seafloor.

Keywords: *Synechococcus*; Cell-clay aggregates; Metal adsorption; Surface complexation

1. INTRODUCTION

Microorganisms and clay minerals rarely exist alone in the natural environment (Ledin, 2000; Zhou and Huang 2001; Zeng et al., 2020). Rather, microorganisms are generally adsorbed to solid surfaces, including clay minerals, as a consequence of attractive van der Waals interactions, hydrogen bonding, hydrophobicity, surface roughness, surface tension and ion bridging (Ledin et al., 1999; Huang et al., 2000; Yee et al., 2000; Huang et al., 2005; Krause et al., 2019; Li et al., 2019). The surface properties of these aggregates differ dramatically from pure bacterial or

* Corresponding author. Fax: +86 022 66229562.
E-mail address: zhouqx@nankai.edu.cn (Q. Zhou).

https://doi.org/10.1016/j.gca.2020.09.002
0016-7037/

mineral surfaces, particularly in terms of surface area and charge, hydrophobicity, double-layer properties, numbers of reactive sites, and potential metal-binding affinity (Neihof and Loeb 1972; Walker et al., 1989; Huang et al., 2005; Chen et al., 2009; Putnis and Ruiz-Agudo, 2013; Martinez et al., 2016; Hirst et al., 2017; Zhou, 2017). Indeed, the presence of microbial coatings can alter the reactivity of the underlying mineral surface through masking of high-energy surface sites, providing a variety of new sites for metal binding and/or modifying the electrical properties of the mineral-water interface (Neihof and Loeb 1972; Templeton et al., 2001, 2003; Phoenix et al., 2002; Wigginton, 2014; Kikuchi et al., 2019; Zeng et al., 2020). It is, therefore, important to consider bacteria-mineral aggregates as a geochemically reactive solids and to quantify their metal scavenging ability as mixed adsorbent systems.

In the past decade, the database pertaining to proton and metals adsorption onto microbial cells and clay minerals has expanded considerably, which when combined with surface complexation modelling (SCM), has allowing for improved predictions of their heavy metal scavenging ability in aquatic environments (Fein et al., 1997; Ueshima et al., 2008; Gu et al., 2010; Mishra et al., 2010; Liu et al., 2015, 2018). Other studies have examined the role of bacteria-clay mineral aggregates in terms of their metal binding. For instance, Walker et al. (1989) observed that *Bacillus subtilis* cell wall-clay and *Escherichia coli* cell wall-clay mixtures bound 20–90% less metal than equal amounts of the individual components did. Transmission electron microscopy and energy-dispersive X-ray spectroscopy confirmed that the adsorption of cells to clay resulted in the masking or neutralization of chemically reactive adsorption sites normally available to metal ions. Huang et al. (2000) reported that the presence of *Rhizobium fredii* increased the Cd adsorption affinity of kaolin (116.5%). Templeton et al. (2001 & 2003) showed that at least 50% of the total bound Pb(II) was associated with the *Burkholderia cepacian* biofilm component at pH < 5.5, and goethite became dominant (70% adsorption) above pH 6.0 in systems exposed to solutions of Pb(II). Kuang et al. (2019) reported that a combination of extracellular polymeric substances (EPS) secreted from *Microcystis aeruginosa* with kaolinite created new adsorption sites, which increased Cu(II) adsorption. The above studies suggest that heavy metals adsorption onto microbe-clay minerals aggregates is not only different than those of the individual constituent components, but aggregation leads to a more complex surface for metal adsorption reactions. Furthermore, the surface reactivity of microbe-clay mineral aggregates is influenced by bacterial species (especially the functionality and composition of cell wall envelopes) and the clay mineral type.

It has been demonstrated that a significant fraction of primary production in the oceans may be attributed to the growth of planktonic cyanobacteria (Fisher, 1985; Flombaum et al., 2013), with some genera, such as *Synechococcus*, reaching densities on the order of 10^4-10^6 cells/mL in the photic zone (Waterbury et al., 1979). Clay minerals are also widely distributed in marginal marine settings; the total suspended sediment delivered by all rivers to the oceans annually is estimated to be 13.5×10^9 tons (Milliman and Meade, 1983), of which 10–25% is clay (Manheim et al., 1970; Schroeder et al., 2015). These clays can serve as significant scavengers for heavy metals, and transport and deposit heavy metals in rivers and estuaries (Liu et al., 2018; Hao et al., 2020). When considering aggregates of cyanobacterial cells and clay minerals as biosorbents for metal binding (Kikuchi et al., 2019), it is important to mimic closely the chemical conditions of seawater. However, such studies are limited to date.

In the present work, we investigated Cd(II) adsorption by mixtures of the marine cyanobacterium *Synechococcus* sp. PCC 7002 (henceforth referred to as *Synechococcus*) and three types of clay minerals: kaolinite, montmorillonite, and illite. We focused on this system because clay minerals and planktonic microorganisms are ubiquitous suspended particulate matter in the oceans, the three clay minerals encompass the range of structural compositions found in nature (1:1 of kaolinite, 2:1 of montmorillonite and illite), and the surface reactivities of the adsorbents have been characterized previously (Liu et al., 2015, 2018). We hypothesized that in systems where a clay mineral and planktonic *Synechococcus* cells were mixed, aggregation would occur to an extent where surface functional group site blockage would lower the observed extent of Cd adsorption versus component additivity (CA) model predictions of sorption, which do not consider site blockage. Further, we hypothesized that the extent of site blockage and reduced Cd adsorption would be considerable at the high ionic strength tested (0.56 M), where clay mineral – bacterial cell aggregation is enhanced, versus previous experiments that used far lower ionic strengths (e.g., Alessi and Fein, 2010). Our systems necessarily have bacterial cells, clay minerals, and Cd concentrations that are higher than expected ones in freshwater, estuarine, or marine conditions; however, aggregation of cells and clay minerals is enhanced at higher sorbent concentrations, allowing us to test whether site blockage is an important factor in reducing Cd sorption to the aggregates. To test the two hypotheses above, there were three aims in this study: (1) determining the morphology and size distribution of the cell-clay mineral aggregates; (2) observing Cd adsorption onto the *Synechococcus*-clay mineral composites; and (3) testing the ability of the CA surface complexation modeling approach to predict Cd adsorption behaviors in various *Synechococcus*-clay mineral aggregates and compare those predictions to observed Cd removal from aqueous solution.

2. MATERIALS AND METHODS

2.1. Preparation of bacterial cells

Cyanobacterial strain *Synechococcus* sp. PCC 7002 was grown and harvested in a manner similar to that described by Liu et al. (2015). The bacteria were inoculated in media A (Stevens and Van Baalen 1973) supplemented with 0.01 M $NaNO_3$ (designated A+ media; Stevens and Porter 1980) and buffered with 1 M Tris at pH 8.2. Stock bacteria were cultured on A+ agar plates at 30 °C. Once

a suitable colony developed on the plate, cells were transferred into 50 mL of A+ media using an inoculation loop to acquire experimental cultures. In order to obtain sufficient biomass, bacteria were transferred to 300 mL cultures. Aeration was provided by constant shaking on an incubator rotator shaker at 150 rpm and while bubbling with filtered and humidified air throughout. Growth was monitored by optical density measurements at 750 nm, and bacteria were harvested at the exponential phase ($OD_{750} = 0.58 \pm 0.03$) by centrifuging the broth at 14,500*g* for 10 min at room temperature to pellet the cells. After decanting the broth, the bacteria were washed four times in 30 mL of 0.56 M NaCl. Between each wash, the bacteria were centrifuged at 8500*g* for 10 min to pellet the bacteria. After the washing cycles, the bacteria were transferred to a weighed centrifuge tube for wet weight determination. The method of preparation described here removes excess growth media and adsorbed cations from the bacterial surface, and renders the bacteria alive, but metabolically inactive.

2.2. Preparation of clay mineral powders

Well crystallized kaolinite (KGa-2), montmorillonite (SWy-2) and illite (IMt-2) were obtained from the Clay Mineral Society (CMS), Source Clays Repository at the University of Purdue, West Lafayette. The three clay minerals were used as the clay sorbents in our systems. Following a procedure similar to that used by Liu et al. (2018), all three types of clay mineral powders were soaked in 1 M NaCl solution that was previously adjusted to pH 3.0 with concentrated HCl for 2 h to remove impurities. The clay was then washed three additional times in acidic 1 M NaCl solutions. After each wash, the supernatant pH was measured, and then the clay suspension was centrifuged at 8100*g* for 10 min to pellet the clay mineral powder. The clay was subsequently washed in non-acidified solutions of NaCl, gradually decreasing ionic strength from 1 M to 0.56 M to saturate clays with Na^+ cations. After three final washes in 0.56 M NaCl, the pH of the supernatant was measured and the clay was oven dried at 65 °C for 48 h, ground and sieved through 100 mesh, and stored in a sealed centrifuge tube for use (Alessi and Fein, 2010). The surface areas (N_2 adsorption) and cation exchange capacity (CEC) of the clays were $23.50 \pm 0.06\ m^2/g$ and 3.3 meq/100 g for kaolinite (KGa-2) (provided by CMS), $31.82 \pm 0.22\ m^2/g$ and 76.4 meq/100 g for Montmorillonite (SWy-2)) (CMS; Ikhsan et al., 2005), and $45\ m^2/g$ and 27 meq/100 g for illite (IMt-2), respectively (Kriaa et al., 2009).

2.3. Zeta potential and particle size measurements

Zeta potential measurements, using a Malvern Instruments Zetasizer Nano Series instrument, were performed to assess the net surface charge properties of *Synechococcus* cells, the individual clay minerals (kaolinite, montmorillonite, and illite), and aggregates of *Synechococcus* cells and clays. The methodology was conducted as previously described by Liu et al. (2015).

Particle size was examined to assess the size distributions of pure *Synechococcus* cells or clays, or *Synechococcus* cells and clay aggregates. To generate two-sorbent composite systems, 0.5 g of *Synechococcus* cells and 0.5 g of each clay mineral separately were mixed in 100 mL of 0.56 M NaCl solution to yield a total concentration of 10 g/L sorbents. To generate a four-sorbent system, 0.25 g of *Synechococcus* cells and 0.25 g of each of the three clay minerals were mixed in 100 mL of 0.56 M NaCl to yield the same 10 g/L total sorbent concentration. Solutions were adjusted to the starting pH (between pH 3.0–9.0, in 1.0 pH unit intervals) using small aliquots of HCl (0.012, 0.12, and 1.2 M) or NaOH (0.019, 0.19, and 1.9 M) and stirring until the pH stabilized. The 0.56 M NaCl solutions without any sorbents were used as controls. Particle size was measured by a Malvern Instruments Zetasizer Nano series instrument. An average of 6 readings for 3 biological replicates were carried out for measurements.

2.4. Transmission/scanning electron microscopy (TEM)

Samples containing 0.5 g of *Synechococcus* cells and 0.5 g of a clay mineral (kaolinite, montmorillonite or illite) were initially exposed to 100 mL (total concentration of 10 g/L sorbents) of 8.9×10^{-6} M Cd solution at pH 8.0. After 24 h of adsorption, the metal-stained aggregate samples were then fixed in 2.5% gluteraldehyde-2% paraformaldehyde overnight at 4 °C, and washed 3 times in 0.1 M phosphate buffer saline (PBS, pH 7.2). After fixation, samples were centrifuged at 14,500*g* for 10 min to remove excess fixative. Then, a drop of the above samples was placed onto a Formvar Carbon coated grids for 30 s and stained with 1% osmium tetroxide (OsO_4 in 0.12 M cacodylate buffer, pH 7.2). A graded ethanol series dehydration process was simplified to limit samples processing that could affect the interaction of the bacteria and clays. A Philips FEI Morgagni 268 Transmission electron microscope (operating at 80 kV) was then used to image the samples.

2.5. Cd adsorption and desorption experiments

Batch Cd adsorption experiments were performed under open atmosphere at initial Cd concentrations of 8.9×10^{-6} M, referred to hereafter as "1 ppm" experiments for simplicity. The Cd stock solution was prepared from a commercial Cd standard solution (1000 mg/L). A small volume of a 100 mg/L Cd stock solution was added to each bacterial suspension, with the amount determined gravimetrically, to achieve the desired Cd concentration. Two-sorbent and four-sorbent systems were generated as described above (in the zeta potential and particle size measurement sections). Blank tests without solid samples were also performed to determine if Cd was lost to the experimental apparatus or by precipitation in the timeframe of the adsorption experiments. While stirring, the bulk suspension then was divided into 10 mL aliquots in polycarbonate test tubes, and small volumes of concentrated HNO_3 or NaOH were used to adjust the pH of each experiment so that a set covered an initial pH range between

approximately 3.0 to 9.0. The pH was measured using a double-junction glass pH electrode (Orion ROSS ultra, filled with 3 M KCl), calibrated with commercial pH buffers (Thermo Fisher Scientific; pH 2.0, 3.0, 4.0, 7.0, and 10.0). The systems were mixed via end-over-end rotation at 40 rpm for 24 h to allow time for equilibration between the Cd and the sorbents, after which the final pH was measured. The experimental systems were then centrifuged at 12,000*g* for 10 min to pellet the solid sorbent, and the supernatant was decanted and filtered through 0.45 um Nylon membranes. The resulting filtered supernatant was acidified using 2 M HCl. The concentration of dissolved Cd remaining in the filtered supernatants was measured using an Inductively Coupled Plasma-Optical Emission Spectrometer (ICP-OES), calibrated with matrix-matched standards (Thermo Fisher Scientific). The analytical uncertainty of the ICP-OES for measuring Cd at experimental concentrations was determined to be ±2% by repeat analysis of standards.

Desorption experiments were carried out by decanting the equilibrated supernatant solution after centrifugation, and adding an equal volume of acidified 0.56 M NaCl solution (pH = 3.0) to each of the samples. After gentle agitation for 24 h, the suspensions were centrifuged and filtered as described previously, and the Cd concentration in the supernatant was measured. The amount of Cd measured was compared to the concentration of Cd adsorbed to calculate the percent of Cd recovered.

2.6. Surface complexation modeling

In this study, we employ a three-site NEM surface complexation approach that includes carboxyl, phosphoryl, and amino sites to model the proton and Cd adsorption behavior to *Synechococcus* cells (Liu et al., 2015), and a two-site NEM surface complexation model, which included both a basal siloxane surface site (≡X^-) and one amphoteric edge site (≡SOH), to describe cation adsorption onto kaolinite, montmorillonite and illite (Liu et al., 2018). Cd activities on *Synechococcus* cells were determined based on the following hypothesized surface adsorption reactions:

$$Cd^{2+} + R - A_i^- \leftrightarrow R - A_i(Cd)^+ \quad (1)$$

Cd-ligand stability constants are defined as:

$$K_{A_i-Cd} = \frac{[R - A_i(Cd)^+]}{[R - A_i^-] \cdot a_{Cd^{2+}}} \quad (2)$$

where $[R - A_i(Cd)^+]$ is the concentration of the Cd-ligand organic complex, $[R - A_i^-]$ is the concentration of ligands and $a_{Cd^{2+}}$ is the activity of Cd^{2+} in solution. The equilibrium constant, K_{A_i-Cd} is reported as log K_{A_i-Cd}.

Cd adsorption on the basal siloxane surface sites (≡X^-) and amphoteric edge site (≡SOH) were based on the following hypothesized adsorption reactions:

$$\equiv X^- \cdot Na^+ + Cd^{2+} \leftrightarrow \equiv X^- \cdot Cd^{2+} + Na^+ \quad (3)$$

$$\equiv SOH^0 + Cd^{2+} \leftrightarrow \equiv SOCd^+ + H^+ \quad (4)$$

The Cd-site stability constant for the above reactions were defined as:

$$K_{XCd} = \frac{[\equiv X^- \cdot Cd^{2+}] \cdot \alpha_{Na^+} \cdot \gamma_{Na^+}}{[\equiv X^- \cdot Na^+] \cdot \alpha_{Cd^{2+}} \cdot \gamma_{Cd^{2+}}} \quad (5)$$

$$K_{SOCd^+} = \frac{[\equiv SOCd^+] \cdot \alpha_{H^+} \cdot \gamma_{H^+}}{[\equiv SOH^0] \cdot \alpha_{Cd^{2+}} \cdot \gamma_{Cd^{2+}}} \exp(-F\psi_{edge}/RT) \quad (6)$$

where $\exp(-F\psi_{edge}/RT)$ is the electrostatic term, F is the Faraday constant (C/mol), ψ is the surface potential (V), R is the gas constant (C/mol/K), and T is the absolute temperature (K). $\psi_{edge} = 0$ for an uncharged edge surface, which was used for the NEM approach.

As described by Liu et al. (2018), both the non-electrostatic model (NEM) and the constant capacitance model (CCM) were successfully developed to describe proton and Cd adsorption onto the single reference clay minerals, the electrostatic term (CCM) is small and could be neglect primarily due to the fact that the diffuse and intermediate potentials are slightly dependent on pH and Cd concentrations. Parameters of the best fitting models are displayed in Table 1. Calculations also considered 6 aqueous Cd hydrolysis reactions, 3 cadmium carbonate complexes, and aqueous cadmium chloride complexes (Table 2) (Zirino and Yamamoto 1972; Baes and Mesmer 1976; Stipp et al., 1993). A component-additivity approach was then used, with bacteria-clay mineral aggregates as adsorbents, to predict Cd adsorption behavior. Models of the *Synechococcus*-clay mineral aggregates use the acidity and equilibrium constants calculated in the SCMs described above and compiled in Table 1 to independently predict the extent of Cd adsorption in each *Synechococcus*-clay mineral aggregate. For the *Synechococcus*-clay mineral aggregates, the computer program FITEQL 4.0 (Westall, 1982) can simulate Cd adsorption to different adsorbent components.

3. RESULTS

3.1. Zeta potential and particle size distribution

The zeta potentials of *Synechococcus* cells, individual clay minerals, and the composite of *Synechococcus* and clay minerals are plotted against pH in Fig. 1. In terms of individual zeta potentials, *Synechococcus* demonstrated a continuous increase in net negative surface charge from pH 4.0 to 6.0, and above which the surface charge remains constant. Kaolinite, montmorillonite and illite also exhibited an increasingly negative surface charge with increasing pH, with montmorillonite being the most anionic over the entire pH range studied, followed by illite and then kaolinite. The presence of kaolinite in composite samples partially neutralized the negative surface charge of *Synechococcus* cells within the tested pH range of 3.0–9.0, but increased the negative surface charge of kaolinite alone. For *Synechococcus*-montmorillonite system, the zeta potential of montmorillonite with *Synechococcus* cells was more negative than *Synechococcus* cells alone, but less negative than montmorillonite alone. In contrast, the addition of illite in *Synechococcus* cells led to diminished negative surface charge of *Synechococcus* or illite alone within the tested pH range of 3.0–9.0.

Table 1
Proton and Cd(II) reactions at *Synechococcus* cell walls, kaolinite, montmorillonite, and illite.

Synechococcus bacterial cells Reaction	[Site][a]	pK_a[b]
$R-A_1(H)^0 \leftrightarrow H^+ + R-A_1^-$	11.70 ± 0.62	5.07 ± 0.03
$R-A_2(H)^0 \leftrightarrow H^+ + R-A_2^-$	5.72 ± 0.22	6.71 ± 0.07
$R-A_3(H)^0 \leftrightarrow H^+ + R-A_3^-$	6.96 ± 0.76	8.54 ± 0.15
	Log K_{Cd}, 1 ppm	
$Cd^{2+} + R-A_1^- \leftrightarrow R-A_1(Cd)^+$	1.15 ± 0.67	
$Cd^{2+} + R-A_2^- \leftrightarrow R-A_2(Cd)^+$	1.78 ± 0.07	
$Cd^{2+} + R-A_3^- \leftrightarrow R-A_3(Cd)^+$	2.74 ± 0.03	
Kaolinite KGa-2		
Reaction	[Site][a]	pK_a[c]
$\equiv SOH^0 \leftrightarrow \equiv SO^- + H^+$	0.26 ± 0.02	8.55 ± 0.10
$\equiv SOH^0 + H^+ \leftrightarrow \equiv SOH_2^+$		-6.01 ± 0.64
$\equiv X^- \cdot H^+ + Na^+ \leftrightarrow \equiv X^- \cdot Na^+ + H^+$	0.43 ± 0.02	4.07 ± 0.02
	Log K_{Cd}, 1 ppm	
$\equiv SOH^0 + Cd^{2+} \leftrightarrow \equiv SOCd^+ + H^+$	2.38	
$\equiv X^- \cdot Na^+ + Cd^{2+} \leftrightarrow \equiv X^- \cdot Cd^{2+} + Na^+$	-1.04	
Montmorillonite SWy-2		
Reaction	[Site][a]	pK_a[c]
$\equiv SOH^0 \leftrightarrow \equiv SO^- + H^+$	0.70 ± 0.05	8.63 ± 0.04
$\equiv SOH^0 + H^+ \leftrightarrow \equiv SOH_2^+$		-5.10 ± 0.06
$\equiv X^- \cdot H^+ + Na^+ \leftrightarrow \equiv X^- \cdot Na^+ + H^+$	0.74 ± 0.05	2.04 ± 0.40
	Log K_{Cd}, 1 ppm	
$\equiv SOH^0 + Cd^{2+} \leftrightarrow \equiv SOCd^+ + H^+$	2.61	
$\equiv X^- \cdot Na^+ + Cd^{2+} \leftrightarrow \equiv X^- \cdot Cd^{2+} + Na^+$	-2.46	
Illite IMt-2		
Reaction	[Site][a]	pK_a[c]
$\equiv SOH^0 \leftrightarrow \equiv SO^- + H^+$	0.20 ± 0.02	8.91 ± 0.18
$\equiv SOH^0 + H^+ \leftrightarrow \equiv SOH_2^+$		-6.43 ± 0.41
$\equiv X^- \cdot H^+ + Na^+ \leftrightarrow \equiv X^- \cdot Na^+ + H^+$	0.53 ± 0.10	3.91 ± 0.24
	Log K_{Cd}, 1 ppm	
$\equiv SOH^0 + Cd^{2+} \leftrightarrow \equiv SOCd^+ + H^+$	2.04	
$\equiv X^- \cdot Na^+ + Cd^{2+} \leftrightarrow \equiv X^- \cdot Cd^{2+} + Na^+$	-1.48	

[a] Concentration of sites, in mmol/g.
[b] Values from Liu et al. (2015).
[c] Values from Liu et al. (2018).

Table 2
Cadmium hydrolysis reactions and cadmium chloride complexes used in the surface complexation modeling.

Hydrolysis reactions[a]	Log K_{Cd}
$Cd^{2+} + H_2O \leftrightarrow CdOH^+ + H^+$	-9.84
$Cd^{2+} + 2H_2O \leftrightarrow Cd(OH)_2(aq) + 2H^+$	-20.03
$Cd^{2+} + 3H_2O \leftrightarrow Cd(OH)_3^- + 3H^+$	-31.70
$Cd^{2+} + 4H_2O \leftrightarrow Cd(OH)_4^{2-} + 4H^+$	-47.83
$2Cd^{2+} + H_2O \leftrightarrow Cd_2(OH)^{3+} + H^+$	-9.66
$4Cd^{2+} + 4H_2O \leftrightarrow Cd_4(OH)_4^{4+} + 4H^+$	-33.33
Chloride complexes [b]	Log K
$Cd^{2+} + Cl^- \leftrightarrow CdCl^+$	2.53
$Cd^{2+} + 2Cl^- \leftrightarrow CdCl_2$	3.49
$Cd^{2+} + 3Cl^- \leftrightarrow CdCl_3^-$	2.89
Cadmium carbonate complexes [c]	Log K
$H_2CO_3 \leftrightarrow H^+ + HCO_3^-$	-6.62
$HCO_3^- \leftrightarrow CO_3^{2-} + H^+$	-10.86
$Cd^{2+} + CO_3^{2-} \leftrightarrow CdCO_3(s)$	13.16

[a] Values from Baes and Mesmer (1976) and were adjusted to ionic strength of 0.56 M using the Davies equation with a 0.2I term.
[b] Values from Zirino and Yamamoto (1972) and were adjusted to ionic strength of 0.56 M using the Davies equation with a 0.2I term.
[c] Values from Stipp et al. (1993) and were adjusted to ionic strength of 0.56 M using the Davies equation with a 0.2I term.

Not surprisingly, the composites of *Synechococcus* and clay minerals had significantly larger particle sizes than the individual clay minerals alone (2300–4900 nm vs. 1200–2000 nm, 2700–8700 nm vs. 1350–4000 nm, and 3300–5400 nm vs. 2200–3000 nm for kaolinite, montmorillonite, and illite, respectively). The mean size of the individual clay particles follows the order of montmorillonite > illite > kaolinite, and the particle sizes of the *Synechococcus*-clay mineral aggregates follows the same order as the individual clay mineral particles. The particle size of *Synechococcus*-montmorillonite aggregates showed a significant increase to over 8000 nm at pH 7.0, with smaller aggregate sizes of between 2800–4300 nm at higher and lower pH. The particle size of *Synechococcus*-supplemented kaolinite aggregates generally decreased with increasing pH, while the particle size of *Synechococcus*-supplemented illite microaggregates increased slowly with the increase in pH.

3.2. Electron microscopic results

TEM analysis of control *Synechococcus* cell without clay minerals revealed that extracellular structures, such as

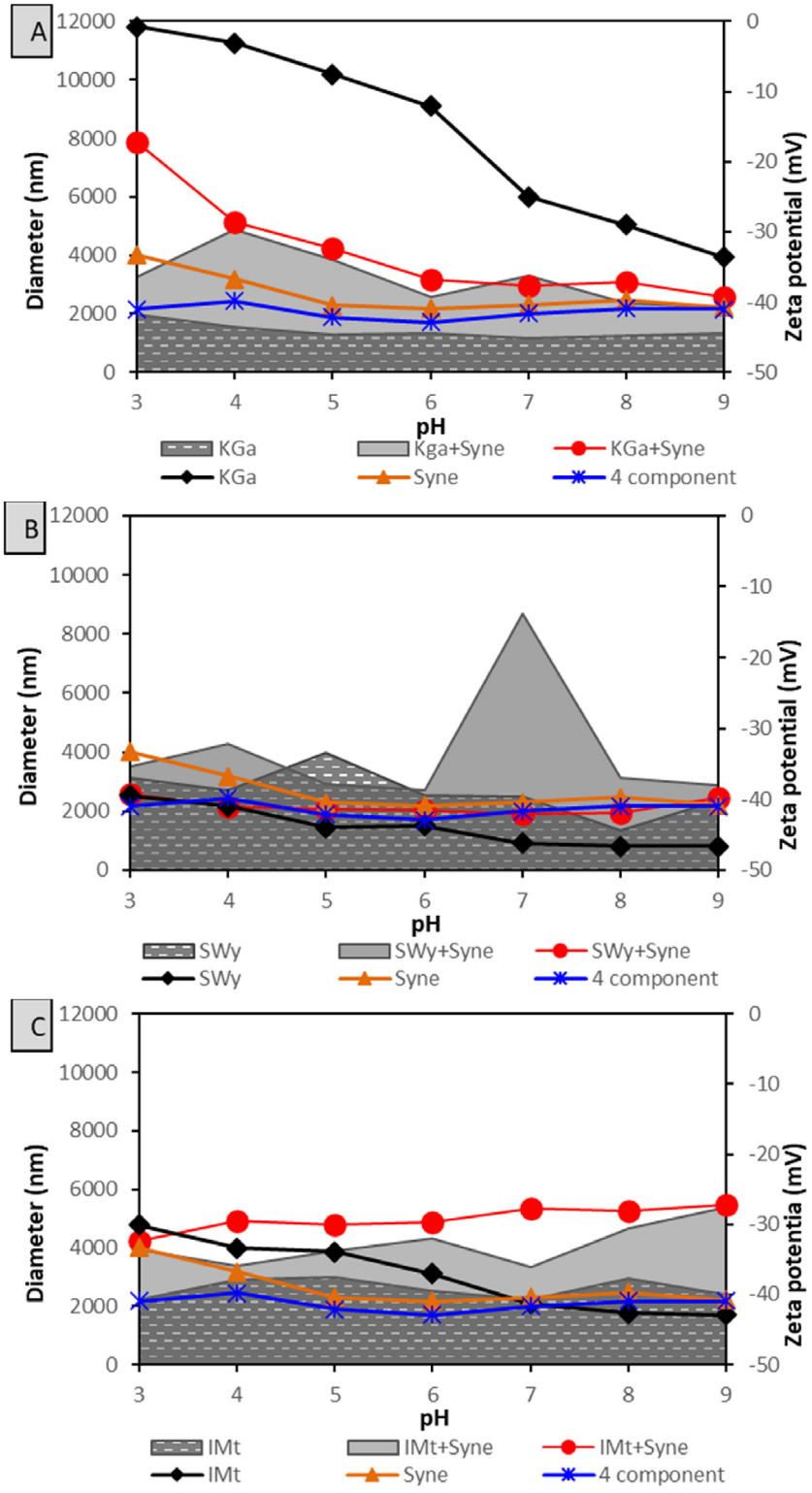

Fig. 1. Trends in zeta potential and particle size across the pH range of 3.0 to 9.0 for clay minerals and *Synechococcus* mixtures: (A) Kaolinite (KGa) - *Synechococcus* (Syne); (B) Montmorillonite (SWy) - *Synechococcus* (Syne); (C) Illite (IMt) – *Synechococcus* (Syne). Light grey filled regions show the particle size of individual clay mineral aggregates, dark grey filled regions show the particle size of clay mineral + *Syne* mixtures, red filled circles indicate the zeta potential of clay mineral + *Syne* mixtures, black filled diamonds show the zeta potential of individual clay minerals, and grey filled triangles indicate the zeta potential of *Syne*.

fimbriae, are clearly visible (Fig. 2A and B). In the aggregates, the *Synechococcus* cells are encrusted with clay minerals (Fig. 2C–J), forming layers around *Synechococcus* cells that can be over 1 μm thick. In *Synechococcus*-kaolinite aggregates, individual hexagonal mineral platelets make tangential edge-to-edge contact, and stacked kaolinite grains form rough and granular aggregates as compared to the smooth surface of encrusted cyanobacterial cell (Fig. 2C and D). In these aggregates, connections between cyanobacterial cells and kaolinite grains are not confined to grain edges only, but involve the faces of grains as well. With respect to montmorillonite and illite, cyanobacterial cells make contact with clay mineral grains along the clay-mineral edge (edge-to-edge contact), as well as the face (edge-to-face contact). *Synechococcus* cells not only bind to the surface but also between the gaps of loose aggregates to form tighter complexes (Fig. 2E-F, G-H). *Synechococcus* cells encased in montmorillonite grains generally exhibit a rosette-type structure (Fig. 2E). The diameters of bacteria-clay mineral aggregates are around 2–5 μm, 2–8 μm, and 3–5 μm for *Synechococcus*-kaolinite, *Synechococcus*-montmorillonite, and *Synechococcus*-illite, respectively. These diameters fall in the range of particle sizes measured using the ZetaSizer.

3.3. Cd adsorption

3.3.1. Cd adsorption to Synechococcus-clay mineral mixtures

The pH edges of Cd adsorption onto *Synechococcus*-clay mineral composites with mass ratios of 1:1 are shown in Fig. 3. The measured extents of Cd adsorption onto the aggregates were compared to predictions of Cd adsorption calculated using the CA surface complexation model.

Experiments containing 50% *Synechococcus* and 50% kaolinite (by mass) exhibit Cd adsorption extent significantly less than that of the 100% *Synechococcus* system, but more than was observed in systems containing 100% kaolinite (Fig. 3A). In this system, Cd preferably binds to the sites on kaolinite surface (>50%) relative to that on *Synechococcus* surface below pH 5.0. However, with increasing pH, *Synechococcus* surface sites became dominant sites for Cd adsorption, contributing around 90% of the potential Cd adsorption sites on a molar basis. By contrast, kaolinite only adsorbed 10% of the Cd. This is unsurprising given that kaolinite has significantly lower site densities than *Synechococcus*. The percent of Cd adsorption decreased in the experiments with aggregates of *Synechococcus* and clay minerals compared to that of *Synechococcus* alone.

Cd adsorption onto mixtures of *Synechococcus* and montmorillonite is depicted in Fig. 3B. Mixtures of 50% *Synechococcus* and 50% montmorillonite adsorbed intermediate amounts of Cd compared to 100% *Synechococcus* (higher sorptive capacity) and 100% montmorillonite (lower sorptive capacity). The results suggest that montmorillonite dominates the adsorption behavior of Cd below pH 4.5; above pH 4.5, *Synechococcus* dominates the Cd adsorption (~85%). Predictive models of the mixtures containing 1 ppm Cd match the experimental data well.

Fig. 3C illustrates Cd adsorption behavior onto the mixture of *Synechococcus* and illite. These data show that 100% *Synechococcus* adsorbs the greatest portion of Cd, followed by the 50% *Synechococcus* and 50% illite mixture, and then the 100% illite adsorption experiments. In experiments containing 50% *Synechococcus* and 50% illite by mass, the bacteria represent more than 80% of the surface sites on a molar basis above pH 5.5, and illite the remaining 20%. Below pH 5.5, illite dominates the Cd adsorption. The predictive model matches the measured extents of adsorption in the *Synechococcus*-illite systems reasonably well.

3.3.2. Cd adsorption to four-component mixtures

In the four-component mixtures of the sorbents, *Synechococcus*, kaolinite, montmorillonite, and illite contribute 32%, 18%, 8%, and 42% of the reactive sites at pH 5.5, respectively. The surface sites on *Synechococcus* became deprotonated with increasing pH, and contributed more binding sites for Cd adsorption, representing 55%, 5%, 9%, and 31% of binding sites at pH 9.0, respectively. The Cd adsorption behavior in the four-component mixtures are also well-predicted by the CA model.

4. DISCUSSION

In seawater, microorganisms and clay particles commonly exist in the form of aggregates (Avnimelech et al., 1982; Verspagen et al., 2006; Kennedy et al., 2014). Microbial cells provide abundant reactive ligands which can deprotonate over a wide range of pH (Beveridge and Graham, 1991; Fein et al., 1997; Cox et al., 1999; Lalonde et al., 2008; Liu et al., 2015). These ligands are capable of binding metal cations and serving as nucleation sites for mineral authigenesis (Konhauser et al., 1994; Clarke et al., 1997; Phoenix et al., 2003). In the same way, clay mineral particles in suspension are attracted to cations because of incomplete substitution of divalent cations for trivalent cations in the octahedral sheet or trivalent cations for tetravalent Si in the tetrahedral sheet, results in excess negative charge that attracts metal cations in aqueous solution (Guenther and Bozelli, 2004; Liu et al., 2018). The adsorption of cations to the clay surface can result in a net-positive surface charge, providing binding sites for bacterial cellular surfaces with negative surface charges (Walker et al., 1989; Konhauser et al., 1998; Guenther and Bozelli 2004).

Despite the evidence that living microorganisms attach to clay mineral grains, the significance of this process in terms of sequestrating contaminants (e.g., heavy metals, organic toxicants, and inorganic substances) is unclear. As suggested by this study, heavy metals adsorption onto aggregates of microorganisms and clay minerals does not necessarily result in additive adsorption behavior toward metals such as Cd. Instead, we show the preferential accumulation of Cd to the clay mineral at acidic pH and to the cell surface of *Synechococcus* at neutral to basic pH in the mixture of *Synechococcus* and clay mineral aggregates. The order of Cd uptake was *Synechococcus* > aggregates of *Synechococcus* plus individual clay minerals > aggregates

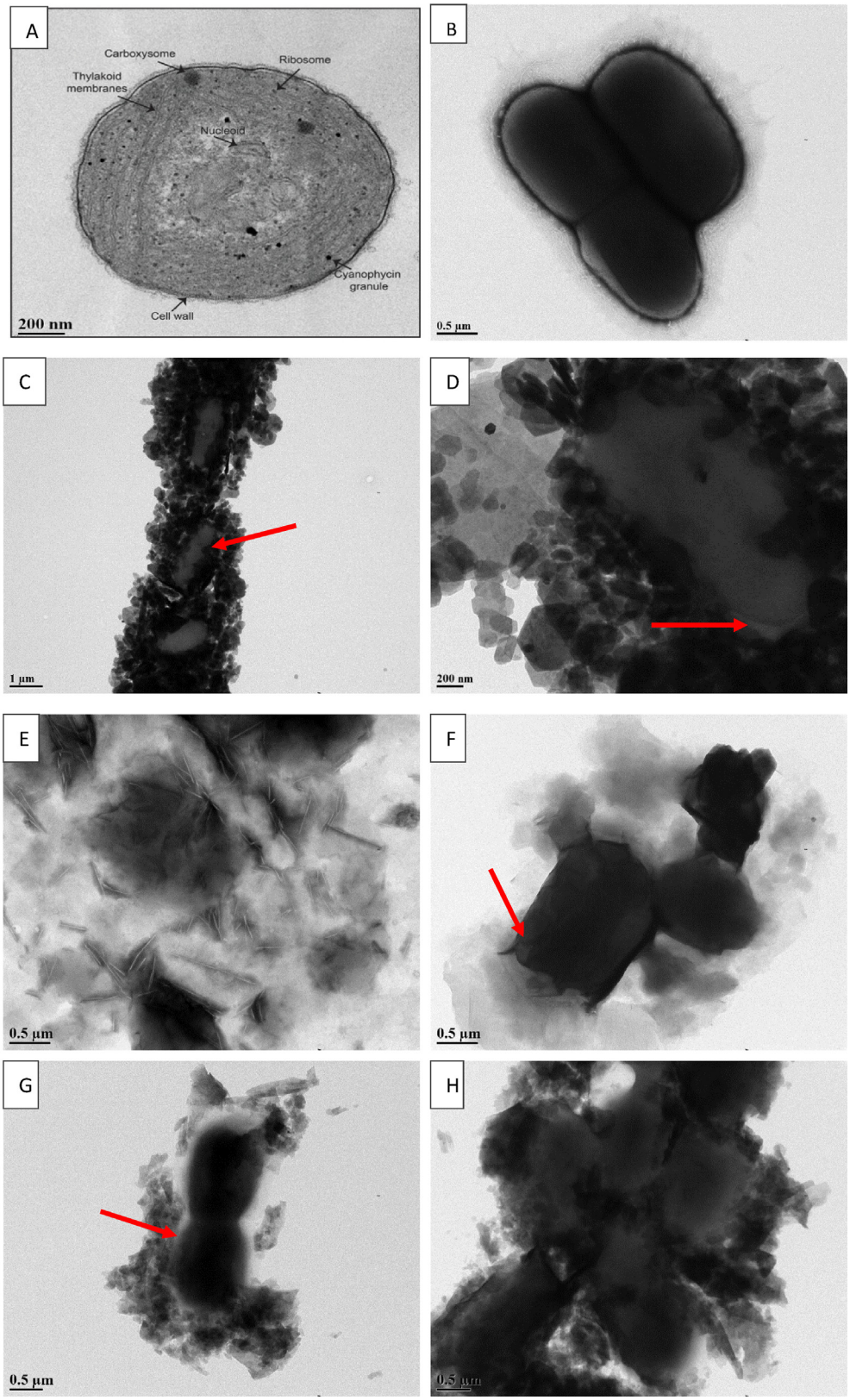

Fig. 2. Transmission electron microscope (TEM) images. (A and B) Control *Synechococcus* cells with no clay present. (C and D) *Synechococcus* cells in the presence of kaolinite. (E and F) *Synechococcus* cells in the presence of montmorillonite. (G and H) *Synechococcus* cells in the presence of illite. (I and J) Mixture of *Synechococcus*, kaolinite, montmorillonite and illite. Red arrows denote the *Synechococcus* cells.

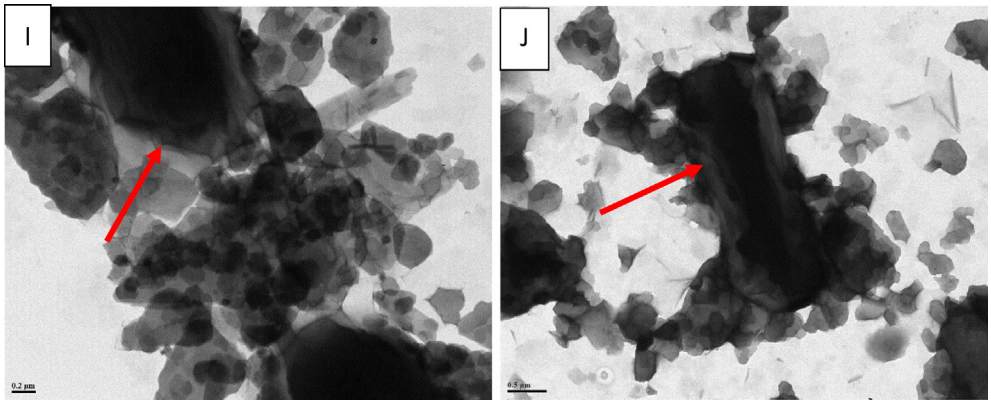

Fig 2. *(continued)*

of *Synechococcus* and 3 clay minerals > individual clay minerals.

Our results are consistent with the limited number of previous studies. For instance, binary mixtures of montmorillonite with either *Bacillus subtilis* (1:1) or *Pseudomonas putida* (1:1) displayed Cd adsorption patterns that are intermediate to individual bacteria and montmorillonite, and an approximately 68%:32% Cd distribution between the bacterial and mineral fraction was found (Du et al., 2017). Alessi and Fein (2010) showed that Cd adsorption decreased systematically with an increasing kaolinite in the *B. subtilis*-kaolinite mixture; 100% *B. subtilis* adsorbs the greatest portion of free Cd, followed by a 75% *B. subtilis* + 25% kaolinite mixture, a 25% *B. subtilis* + 75% kaolinite mixture, and a 100% kaolinite adsorption experiment. Although the majority of Cd adsorption below pH 4.0 is predicted to occur onto permanent structural sites ($\equiv X^-$) of kaolinite (Hao et al., 2019), *B. subtilis* contributes most of the reactive sites for Cd adsorption in *B. subtilis*-kaolinite mixtures (Alessi and Fein 2010). Similarly, Kulczycki et al. (2005) showed that the Cd adsorption capacity of *B. subtilis*-ferrihydrite or *Escherichia coli*-ferrihydrite composites was lower than that of ferrihydrite alone, and that the ferrihydrite surface properties dominate the net surface charge of the bacteria-ferrihydrite composite system with a lesser contribution from the bacteria.

The surface complexation modelling (SCM) approach has proven useful in the prediction of metal adsorption onto minerals and natural organic matter. In multi-adsorbent systems, two surface complexation modeling approaches can be used to describe metal distribution: the general composite (GC) approach and the component additivity approach (Davis et al., 1998). The GC approach uses generic, bulk binding reactions for a geologic matrix as a whole, and does not distinguish the importance of individual adsorbents. Thus, the GC model requires matrix-specific calibration in order to apply it to systems containing differing ratios of the component adsorbents, and thus its extrapolative and predictive capabilities are limited (Goldberg, 2014; Fisher-Power et al., 2019; Johnson et al., 2019). In contrast, the CA approach use binding constants and the relative concentrations of binding sites that have been independently calculated for each matrix component to predict the extent of adsorption in multi-sorbent systems. The CA approach is only valid if the adsorbing solutes have access to all surfaces, and sorbents do not interact with each other (Alessi and Fein, 2010; Dong et al., 2012). Thus, although more challenging to apply, the CA approach enables independent predictions of the extent of adsorption that occurs in complex multi-sorbent systems. The CA approach has been applied successfully in the prediction of metal adsorption on a variety of composites (Pagnanelli et al., 2006; Alessi and Fein, 2010; Johnson et al., 2019).

As is shown in Fig. 3, the experimental sorption data for the *Synechococcus*-mineral aggregates are identical to CA predicted values, which means CA approach could successfully predict Cd adsorption to mixtures of bacterial and clay mineral adsorbents. The CA data indicate that at acidic pH, Cd adsorption is dominated by complexation to clay minerals, despite the excess of reactive sites within the *Synechococcus* biomass. This result suggests that the highly reactive mineral surface sites seem to have not been blocked during bacteria-clay aggregation formation. Our experiments use clay minerals and planktonic cell concentrations that are higher than normally occurred ones in natural environments. At these higher concentrations, clay-cell aggregation should be enhanced, particularly at the relatively high ionic tested in our experiments. Thus if a reduction in Cd removal from solution is not observed in our experiments, where we would expect site blockage to be enhanced, we do not predict that it would impact Cd adsorption at estuarine or marine conditions where clay minerals and planktonic cell concentrations are considerably lower. However, additional binding mechanisms might be involved in the multi-sorbent systems. Firstly, biomass biomineralization processes would be critically important in heavy-metal sequestration. For example, localized metabolic activities might enhance mineral dissolution and the release of Al^{3+} (Konhauser et al., 1998), or potentially induce precipitation with ligands such as PO_4^{3-}, which might ultimately lead to the formation of insoluble, mixed metal phases (Costerton et al., 1995; Templeton et al., 2001; Morin et al., 2001). Second, there are possible transformations of Cd-carboxyl and Cd-phosphate coordination complexes when bacteria are mixed with clay minerals. For example, the bidentate ($\equiv(R\text{-}COO)_2Cd^0$) species may transform to the monodentate ($\equiv R\text{-}COOCd^+$) species.

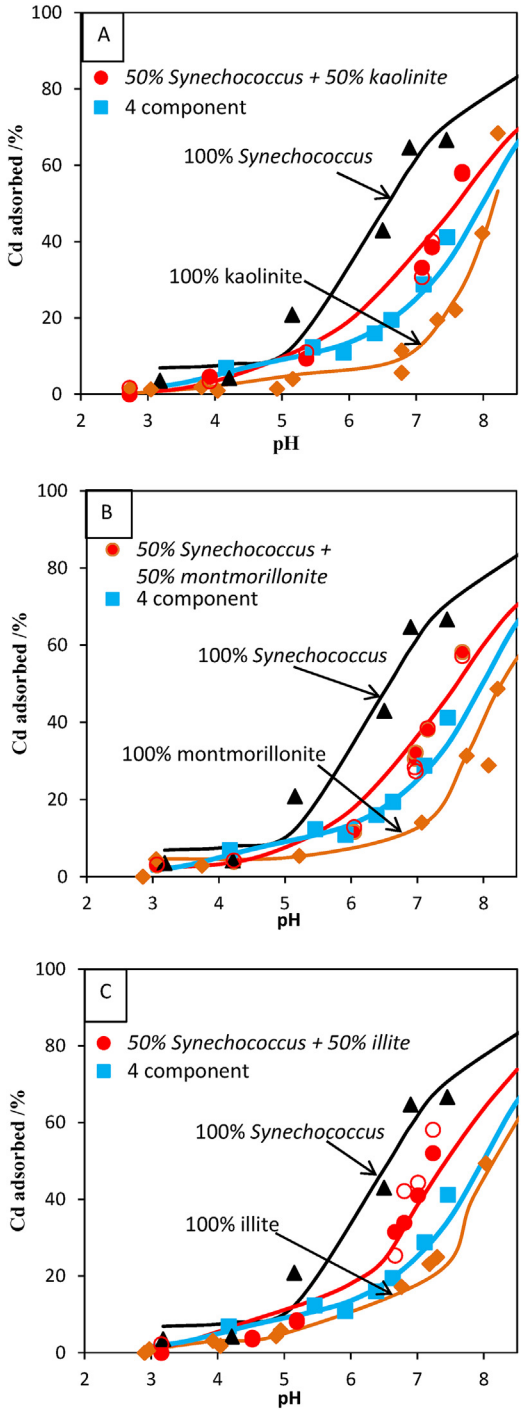

Fig. 3. Adsorption of Cd to clay minerals and *Synechococcus* mixtures: (A) kaolinite + *Synechococcus*; (B) montmorillonite + *Synechococcus*; and (C) illite + *Synechococcus*. Filled diamonds represent individual clay mineral, filled triangles represent single *Synechococcus*, red filled circles represent clay minerals + *Synechococcus* mixtures, blue filled squares represent the four component mixtures, black lines represent the non-electrostatic surface complexation model fits, orange lines represent the non-electrostatic surface complexation model fits for individual clay minerals, and red and blue lines represent the component additivity surface complexation model predictions for two component and four component mixtures, respectively.

Since the latter is positively charged, it may promote bridging between the negatively-charged bacteria and Cd-loaded clay minerals. In this coordination, Cd ions would be complexed by fewer carboxyl or phosphate groups, and thus fewer water molecules would be released from inner-sphere adsorption sites (Du et al., 2017). This additional molecular binding mechanism might result in an underestimation of metal cation distribution onto the bacterial-clay mineral aggregates.

The particles size analyses and TEM images reveal that the addition of cyanobacterial cells leads to significantly larger mean aggregate sizes than for corresponding abiotic controls. The size and composition of these aggregates is dependent on the ratio of bacteria:clay minerals (Johnson et al., 2019). However, the changes in the microtopography did not show an obvious spatial relationship to surface charge or Cd^{2+} adsorption. Previous studies showed that microbial cells can become entrained in settling clay mineral aggregates and then flocculate rapidly (Sengco et al., 2001; Verspagen et al., 2006; Du et al., 2009). As reported by Playter et al. (2017), cyanobacterial cells enhance clay sedimentation significantly, and at a rate that increases with clay concentrations. With an increasing fraction of clay minerals, Cd and heavy metals settles much faster with bacteria under similar supersaturation. A combination of rapid sedimentation and clay mineral encrustation ultimately will not only enhance the preservation potential of this organic matter, but it also means that some of the trace metals incorporated into the sediment pile were derived from cell-clay aggregation in the overlying water column (Playter et al., 2017).

In the specific example of Cd binding to *Synechococcus* – clay aggregates, our work further demonstrates that the relative ratio between planktonic cells and various clay minerals will determine the amount of metal sedimentation, and in our specific example, the incorporation of Cd into the marine sediment record. The significance of these findings can easily be imagined, if we consider that other metals will similarly be transferred from the water column to the sediment pile in the form of cyanobacteria-clay aggregates. Indeed, trace elements are enriched in organic-rich, marine shale deposits – the lithified version of mud - in two ways: (1) by association with organic matter, or (2) by adsorption to the detrital clay fraction and other mineral components. In the former instance, numerous studies support the idea that the burial of redox-sensitive metals scaled with carbon fluxes (Algeo and Maynard, 2004; Reinhard et al., 2013). After organic matter degradation, these elements are liberated into sediment pore-waters, and then incorporated into pyrite under reducing conditions (Xu et al., 2012). In the case of the latter, siliciclastic constituents (e.g., detrital clays) can also import trace elements (Breit and Wanty, 1991; Kelly et al., 2013), with the magnitude of clay-metal enrichment identifiable through cross-plotting elements of interest versus Al or Ti, and then comparing the ratios with average published shale values (Piper and Perkins, 2004; Tribovillard et al., 2006). Most recently, Playter et al. (2017) suggested that aggregates of microbes and clay minerals be considered as trace metal vectors in depositional environments where cyanobacterial blooms could occur in

addition to supply regular clays, such as an estuary or other coastal regions.

However, in order to accurately extrapolate the effectiveness of cyanobacterial cell-clay mineral aggregates as a shuttle for heavy metals to the seafloor, a number of uncertainties need to be constrained. First, the contributions of organic versus inorganic metal cation species to metal sedimentation rates should be determined; similar work is currently being applied to parsing out the amount of metals supplied by planktonic bacteria versus iron-rich minerals for chemical sediments such as banded iron formations (Konhauser et al., 2018). Second, the ability of the cyanobacterial cell-clay mineral microaggregates to bind a wider spectrum of elements from surface water columns should be assessed, including determination of competitive adsorption effects between Cd and other metals or elements. Third, current research shows that the adsorption of Cd onto clay mineral can be transient because metal adsorption onto clay mineral surfaces can be altered by changes in aqueous conditions such as pH and ionic strength (Hao et al., 2020). Specifically, if Cd was previously adsorbed to clay minerals in a freshwater setting (e.g., river) but then carried as suspended sediment to the oceans, the change in aqueous conditions as those sediments transition from estuaries to coastal settings can lead to the desorption of Cd back into the water column. Therefore, the ratio of cells (where Cd is more fixed due to stronger adsorption) versus clays (where Cd is exchangeable) come to be an important, but overlooked determinant in Cd incorporation into the sediment pile.

5. CONCLUSION

In this study, we observed that *Synechococcus* cells accumulate on clay mineral surfaces, promoting the development of larger microaggregates. In *Synechococcus*-clay mineral mixture systems, Cd preferably adsorbs to the *Synechococcus* surface relative to the sites on the clay mineral surfaces. Using Cd stability constants calculated for each sorbent, the CA surface complexation modelling approach provides reasonable predictions of Cd adsorption onto *Synechococcus*-clay composites. Future studies are necessary to explore potential structural changes in clay minerals at different stages of microorganism growth and metabolism, metals fixation and preservation properties onto these microaggregates, and the effects of metals competition for surface functional groups in multi-metal systems.

Declaration of Competing Interest

The authors declare that they have no known competing financial interests or personal relationships that could have appeared to influence the work reported in this paper.

ACKNOWLEDGEMENTS

This work was financially supported by the National Natural Science Foundation of China as a general project (grant No. 21677080) and a Shandong joint project (grant No. U1906222), the Ministry of Education, People's Republic of China as a 111 program (grant No. T2017002), and the Fundamental Research Funds for the Central Universities (ZX20180412). This work was also supported by NSERC Discovery Grants to KOK (RGPIN-165831) and DSA (RGPIN-04134).

APPENDIX A. SUPPLEMENTARY MATERIAL

Supplementary data to this article can be found online at https://doi.org/10.1016/j.gca.2020.09.002.

REFERENCES

Alessi D. S. and Fein J. B. (2010) Cadmium adsorption to mixtures of soil components: Testing the component additivity approach. *Chem. Geol.* **270**, 186–195.

Algeo T. J. and Maynard J. B. (2004) Trace-element behavior and redox facies in core shales of Upper Pennsylvanian Kansas-type cyclothems. *Chem. Geo.* **206**, 289–318.

Avnimelech Y., Troeger B. W. and Reed L. W. (1982) Mutual flocculation of algae and clay: evidence and implications. *Science* **216**(4541), 63–65.

Baes C. F. and Mesmer R. E. (1976) *Hydrolysis of Cations*. Wiley Interscience Publication, New York, USA.

Beveridge T. J. and Graham L. L. (1991) Surface layers of bacteria. *Microbiol. Rev.* **55**, 684–705.

Breit G. N. and Wanty R. B. (1991) Vanadium accumulation in carbonaceous rocks: a review of geochemical controls during deposition and diagenesis. *Chem. Geo.* **91**, 83–97.

Chen X., Hu S., Shen C., Dou C., Shi J. and Chen Y. (2009) Interaction of *Pseudomonas putida* CZ1 with clays and ability of the composite to immobilize copper and zinc from solution. *Bioresour. Technol.* **100**, 330–337.

Clarke W. A., Konhauser K. O., Thomas J. C. and Bottrell S. H. (1997) Ferric hydroxide and ferric hydroxysulfate precipitation by bacteria in an acid mine drainage lagoon. *FEMS Microbiol. Rev.* **20**(3–4), 351–361.

Costerton J. W., Lewandowski Z., Caldwell D., Korber D. and Lappin-Scott H. (1995) Microbial biofilms. *Annu. Rev. Microbiol.* **49**, 711–745.

Cox J. S., Smith D. S., Warren L. A. and Ferris F. G. (1999) Characterizing heterogeneous bacterial surface functional groups using discrete affinity spectra for proton binding. *Environ. Sci. Technol.* **33**, 4514–4521.

Davis J., Coston J., Kent D. and Fuller C. (1998) Application of the surface complexation concept to complex mineral assemblages. *Environ. Sci. Technol.* **32**, 2820–2828.

Dong W., Tokunaga T. K., Davis J. A. and Wan J. (2012) Uranium(VI) adsorption and surface complexation modeling onto background sediments from the F-area Savannah River site. *Environ. Sci. Technol.* **46**, 1565–1571.

Du H. H., Qu C. C., Liu J., Chen W. L., Cai P., Shi Z. H., Yu X. Y. and Huang Q. Y. (2017) Molecular investigation on the binding of Cd(II) by the binary mixtures of montmorillonite with two bacterial species. *Environ. Pollut.* **229**, 871–878.

Du J. H., Pushkarova R. A. and Smart R. S. C. (2009) A cryo-SEM study of aggregate and floc structure changes during clay settling and raking processes. *Int. J. Miner. Process* **93**, 66–72.

Fein J. B., Daughney C. J., Yee N. and Davis T. A. (1997) A chemical equilibrium model for metal adsorption onto bacterial surfaces. *Geochim. Cosmochim. Acta* **61**, 3319–3328.

Fisher-Power L. M., Shi Z. Q. and Cheng T. (2019) Testing the "component additivity" approach for modelling Cu and Zn adsorption to a natural sediment. *Chem. Geol.* **512**, 31–42.

Fisher N. (1985) Accumulation of metals by marine picoplankton. *Mar. Biol.* **87**, 137–142.

Flombaum P., Gallegos J. L., Gordillo R. A., Rincón J., Zabala L. L., Jiao N., Karl D. M., Li W. K., Lomas M. W. and Veneziano D. (2013) Present and future global distributions of the marine Cyanobacteria *Prochlorococcus* and *Synechococcus*. *Proc. Natl. Acad. Sci. USA* **110**, 9824–9829.

Goldberg S. (2014) Application of surface complexation models to anion adsorption by natural materials. *Environ. Toxicol. Chem.* **33**, 2172–2180.

Gu X., Evans L. J. and Barabash S. J. (2010) Modeling the adsorption of Cd (II), Cu (II), Ni (II), Pb (II) and Zn (II) onto montmorillonite. *Geochim. Cosmochim. Acta* **74**, 5718–5728.

Guenther M. and Bozelli R. (2004) Factors influencing algae-clay aggregation. *Hydrobiologia* **523**, 217–223.

Hao W., Pudasainee D., Gupta R., Kashiwabara T., Alessi D. S. and Konhauser K. O. (2019) Effect of acidic conditions on surface properties and metal binding capacity of clay minerals. *ACS Earth Space Chem.* **3**, 2421–2429.

Hao W., Kashiwabara T., Jin R., Takahashi Y., Gingras M. K., Alessi D. S. and Konhauser K. O. (2020) Clay minerals as a source of cadmium to estuaries. *Sci. Rep.* **10**, 10417.

Hirst C., Andersson P. S., Shaw S., Burke I. T. and Porcelli D. (2017) Characterisation of Fe-bearing particles and colloids in the Lena River basin, NE Russia. *Geochim. Cosmochim. Acta* **213**, 553–573.

Huang Q., Chen W. and Xu L. (2005) Adsorption of copper and cadmium by Cu- and Cd-resistant bacteria and their composites with soil colloids and kaolinite. *Geomicrobiol. J.* **22**, 227–236.

Huang Q., Wu J., Chen W. and Li X. (2000) Adsorption of cadmium by soil colloids and minerals in presence of rhizobia. *Pedosphere* **10**, 299–307.

Ikhsan J., Wells J. D., Johnson B. B. and Angove M. J. (2005) Surface complexation modeling of the sorption of Zn (II) by montmorillonite. *Colloids Surf. A Physicochem. Eng. Asp.* **252**, 33–41.

Johnson C. R., Hopf J., Shrout J. D. and Fein J. B. (2019) Testing the component additivity approach to surface complexation modeling using a novel cadmium-specific fluorescent probe technique. *J. Colloid Interface Sci.* **534**, 683–694.

Kelly K. D., Benzel W. M., and Pfaff K. (2013) Preliminary mineralogy and geochemistry of metal-rich (Mo-Ni-V-Zn) oil shale of the Carboniferous Heath Formation, Montana, USA. In: Mineral Deposit Research for a High-Tech World, 12th SGA Biennial Meeting 2013. Proceedings (E. Jonsson ed.), vol. 2, pp. 636–639.

Kennedy M. J., Lohr S. C., Fraser S. A. and Baruch E. T. (2014) Direct evidence for organic carbon preservation as clay-organic nanocomposites in a Devonian black shale: from deposition to diagenesis. *Earth Planet. Sci. Lett.* **388**, 59–70.

Kikuchi S., Kashiwabara T., Shibuya T. and Takahashi Y. (2019) Molecular-scale insights into differences in the adsorption of cesium and selenium on biogenic and abiogenic ferrihydrite. *Geochim. Cosmochim. Acta* **251**, 1–14.

Konhauser K. O., Fyfe W. S., Schultze-Lam S., Ferris F. G. and Beveridge T. J. (1994) Iron phosphate precipitation by epilithic microbial biofilms in Arctic Canada. *Can. J. Earth Sci.* **31**, 1320–1324.

Konhauser K. O., Fisher Q. J., Fyfe W. S., Longstaffe F. J. and Powell M. A. (1998) Authigenic mineralization and detrital clay binding by freshwater biofilms: The Brahmani River, India. *Geomicrobiol. J.* **15**, 209–222.

Konhauser K. O., Robbins L. J., Alessi D. S., Flynn S. L., Gingras M. K., Martinez R. E., Kappler A., Swanner E. D., Li Y. L., Crowe S. A., Planavsky N. J., Reinhard C. T. and Lalonde S. V. (2018) Phytoplankton contributions to the trace-element composition of Precambrian banded iron formations. *Geol. Soc. Am. Bull.* **130**, 941–951.

Krause L., Biesgen D., Treder A., Schweizer S. A., Klumpp E., Knief C. and Siebers N. (2019) Initial microaggregate formation: Association of microorganisms to montmorillonite-goethite aggregates under wetting and drying cycles. *Geoderma* **351**, 250–260.

Kriaa A., Hamdi N. and Srasra E. (2009) Proton adsorption and acid-base properties of Tunisian illites in aqueous solution. *J. Struct. Chem.* **50**, 273–287.

Kuang X. L., Peng L., Chen A. W., Zeng Q. R., Luo S. and Shao J. H. (2019) Enhancement mechanisms of copper(II) adsorption onto kaolinite by extracellular polymeric substances of *Microcystis aeruginosa* (cyanobacterium). *Int. Biodeterior. Biodegradation* **138**, 8–14.

Kulczycki E., Fowle D., Fortin D. and Ferris F. (2005) Sorption of cadmium and lead by bacteria–ferrihydrite composites. *Geomicrobiol. J.* **22**, 299–310.

Lalonde S. V., Smith D. S., Owttrim G. W. and Konhauser K. O. (2008) Acid–base properties of cyanobacterial surfaces. II: Silica as a chemical stressor influencing cell surface reactivity. *Geochim. Cosmochim. Acta* **72**, 1269–1280.

Ledin M. (2000) Accumulation of metals by microorganisms - processes and importance for soil systems. *Earth-Sci. Rev.* **51**(1–4), 1–31.

Ledin M., Krantz-Rülcker C. and Allard B. (1999) Microorganisms as metal sorbents: comparison with other soil constituents in multi-compartment systems. *Soil Biol. Biochem.* **31**, 1639–1648.

Li G. L., Zhou C. H., Fiore S. and Yu W. H. (2019) Interactions between microorganisms and clay minerals: New insights and broader applications. *Appl. Clay Sci.* **177**, 91–113.

Liu Y. X., Flynn S. L., Alessi D. S., Alam M. S., Hao W., Gingras M. K., Zhao H. and Konhauser K. O. (2018) Acid-base properties of kaolinite, montmorillonite and illite at marine ionic strength. *Chem. Geol.* **483**, 191–200.

Liu Y. X., Alessi D. S., Owttrim G. W., Petrash D. A., Mloszewska A. M., Lalonde S. V., Martinez R. E., Zhou Q. and Konhauser K. O. (2015) Cell surface reactivity of *Synechococcus* sp. PCC 7002: implications for metal sorption from seawater. *Geochim. Cosmochim. Acta* **169**, 30–44.

Manheim F. T., Meade R. H. and Bond G. C. (1970) Suspended matter in surface waters of the Atlantic continental margin from Cape Cod to the Florida Keys. *Science* **167**(3917), 6.

Martinez R. E., Konhauser K. O., Paunova N., Wu W. F., Alessi D. S. and Kappler A. (2016) Surface reactivity of the anaerobic phototrophic Fe(II)-oxidizing bacterium *Rhodovulum iodosum*: Implications for trace metal budgets in ancient oceans and banded iron formations. *Chem. Geol.* **442**, 113–120.

Milliman J. D. and Meade R. H. (1983) World-wide delivery of river sediment to the oceans. *J. Geol.* **91**(1), 1–21.

Mishra B., Boyanov M., Bunker B. A., Kelly S. D., Kemner K. M. and Fein J. B. (2010) High-and low-affinity binding sites for Cd on the bacterial cell walls of *Bacillus subtilis* and *Shewanella oneidensis*. *Geochim. Cosmochim. Acta* **74**(15), 4219–4233.

Morin G., Juillot F., Ildefonse P., Calas G., Samama J., Chevallier, , P. and Brown G. (2001) Mineralogy of lead in a soil developed on a Pb-mineralized sandstone (Largentière, France). *Am. Mineral.* **86**, 92–104.

Neihof R. A. and Loeb G. I. (1972) The surface charge of particulate matter in seawater. *Limnol. Oceanogr.* **17**, 7–16.

Pagnanelli F., Bornoroni L., Moscardini E. and Toro L. (2006) Non-electrostatic surface complexation models for protons and lead (II) sorption onto single minerals and their mixture. *Chemosphere* **63**, 1063–1073.

Phoenix V. R., Martinez R. E., Konhauser K. O. and Ferris F. G. (2002) Characterization and implications of the cell surface

reactivity of *Calothrix* sp. Strain KC97. *App. Environ. Microbiol.* **68**, 4827–4834.

Phoenix V. R., Konhauser K. O. and Ferris F. G. (2003) Experimental study of iron and silica immobilization by bacteria in mixed Fe-Si systems: implications for microbial silicification in hot springs. *Can. J. Earth Sci.* **40**, 1669–1678.

Piper D. Z. and Perkins R. B. (2004) A modern vs. Permian black shale-the hydrography, primary productivity, and water-column chemistry of deposition. *Chem. Geo.* **206**, 177–197.

Playter T., Konhauser K., Owttrim G., Hodgson C., Warchola T., Mloszewska A. M., Sutherland B., Bekker A., Zonneveld J. P., Pemberton S. G. and Gingras M. (2017) Microbe-clay interactions as a mechanism for the preservation of organic matter and trace metal biosignatures in black shales. *Chem. Geol.* **459**, 75–90.

Putnis C. V. and Ruiz-Agudo E. (2013) The mineral–water interface: Where minerals react with the environment. *Elements* **9**, 177–182.

Reinhard C. T., Planavsky N. J., Robbins L. J., Partin C. A., Gill B. C., Lalonde S. V., Bekker A., Konhauser K. O. and Lyons T. W. (2013) Proterozoic ocean redox and biogeochemical stasis. *Proc. Natl. Acad. Sci. USA* **110**, 5357–5362.

Schroeder A., Wiesner M. G. and Liu Z. (2015) Fluxes of clay minerals in the South China Sea. *Earth Planet. Sci. Lett.* **430**, 13.

Sengco M. R., Li A. S., Tugend K., Kulis D. and Anderson D. M. (2001) Removal of red- and brown-tide cells using clay flocculation. I. Laboratory culture experiments with Gymnodinium breve and Aureococcus anophagefferens. *Mar. Ecol. Prog. Ser.* **210**, 41–53.

Stevens S. and Van Baalen C. (1973) Characteristics of nitrate reduction in a mutant of the blue-green alga *Agmenellum quadruplicatum*. *Plant Physiol.* **51**, 350–356.

Stevens S. E. and Porter R. D. (1980) Transformation in *Agmenellum quadruplicatum*. *Proc. Natl. Acad. Sci. U.S.A.* **77**, 6052–6056.

Stipp S. L., Parks G. A., Nordstrom D. K. and Leckie J. O. (1993) Solubility-product constant and thermodynamic properties for synthetic otavite, $CdCO_3$(s), and aqueous association constants for the Cd (II)-CO_2-H_2O system. *Geochim. Cosmochim. Acta* **57**, 2699–2713.

Templeton A. S., Trainor T. P., Traina S. J., Spormann A. M. and Brown G. E. (2001) Pb(II) distributions at biofilm-metal oxide interfaces. *Proc. Natl. Acad. Sci. USA* **98**, 11897–11902.

Templeton A. S., Spormann A. M. and Brown G. E. (2003) Speciation of Pb(II) sorbed by *Burkholderia cepacia*/goethite composites. *Environ. Sci. Technol.* **37**, 2166–2172.

Tribovillard N., Algeo T. J., Lyons T. and Riboulleau A. (2006) Trace metals as paleoredox and paleoproductivity proxies: an update. *Chem. Geo.* **232**, 12–32.

Ueshima M., Ginn B. R., Haack E. A., Szymanowski J. E. S. and Fein J. B. (2008) Cd adsorption onto *Pseudomonas putida* in the presence and absence of extracellular polymeric substances. *Geochim. Cosmochim. Acta* **72**, 5885–5895.

Verspagen J. M. H., Visser P. M. and Huisman J. (2006) Aggregation with clay causes sedimentation of the buoyant cyanobacteria *Microcystis* spp. *Aquat. Microb. Ecol.* **44**, 165–174.

Walker S., Flemming C., Ferris F., Beveridge T. and Bailey G. (1989) Physicochemical interaction of *Escherichia coli* cell envelopes and *Bacillus subtilis* cell walls with two clays and ability of the composite to immobilize heavy metals from solution. *Appl. Environ. Microbiol.* **55**, 2976–2984.

Waterbury J. B., Watson S. W., Guillard R. R. L. and Brand L. E. (1979) Widespread occurrence of a unicellular, marine, planktonic, cyanobacterium. *Nature* **277**(5694), 293–294.

Westall J. C. (1982) *FITEQL: A Computer Program for Determination of Chemical Equilibrium Constants from Experimental Data*. Oregon State University, Department of Chemistry.

Wigginton N. S. (2014) Monitoring the mineral-water interface. *Science* **346**(6209), 597.

Xu L., Lehmann B., Mao J., Nägler T. F., Neubert N., Böttcher M. E. and Escher P. (2012) Mo isotope and trace element patterns of Lower Cambrian black shales in South China: multi-proxy constraints on the paleoenvironment. *Chem. Geo.* **318–319**, 45–59.

Yee N., Fein J. B. and Daughney C. J. (2000) Experimental study of the pH, ionic strength, and reversibility behavior of bacteria–mineral adsorption. *Geochim. Cosmochim. Acta* **64**, 609–617.

Zeng Q., Huang L., Ma J., Zhu Z. and Dong H. (2020) Bioreduction of ferrihydrite-montmorillonite-organic matter complexes: Effect of montmorillonite and fate of organic matter. *Geochim. Cosmochim. Acta* **276**, 327–344.

Zhou Q. (2017) *Ecological Geosciences*. Science Press, Beijing, China.

Zhou Q. and Huang G. (2001) *Environmental Biogeochemistry and Global Environmental Changes*. Science Press, Beijing, China.

Zirino A. and Yamamoto S. (1972) A pH-dependent model for the chemical speciation of copper, zinc, cadmium, and lead in seawater. *Limnol. Oceanogr.* **17**, 661–671.

Associate editor: Mario Villalobos